AIP | Journal of Applied Physics

Strain in free standing CdSe/CdS core-shell nanorods

F. Rajadell, M. Royo, and J. Planelles

Citation: J. Appl. Phys. **111**, 014303 (2012); doi: 10.1063/1.3673256
View online: http://dx.doi.org/10.1063/1.3673256
View Table of Contents: http://jap.aip.org/resource/1/JAPIAU/v111/i1
Published by the American Institute of Physics.

Strain in free standing CdSe/CdS core-shell nanorods

F. Rajadell, M. Royo, and J. Planelles[a)]
Departament de Química Física i Analítica, Universitat Jaume I, E-12080 Castelló, Spain

(Received 1 July 2011; accepted 28 November 2011; published online 3 January 2012)

The main characteristic strain trends in free-standing II–VI wurtzite semiconductor nanorods coated with a few-monolayers shell are reported. Calculations for different aspect ratios and shell thicknesses show that these are key factors for the strength of strain components that can even change their sign. Strain in core-shell nanorods with few monolayers coating is strong and qualitatively different from that of buried dots. Hexagonal symmetry compared to cubic and isotropic approximations reveals that, with the appropriate parameters, isotropic strain mimics very well the strain distributions of wurtzite core-shell nanorods. © *2012 American Institute of Physics*. [doi:10.1063/1.3673256]

I. INTRODUCTION

In the last decade, various colloidal chemical approaches have been successfully developed for synthesizing inorganic nanostructures with controlled morphologies and patterns,[1] so nowadays, semiconductor quantum dots (QDs) are commonly fabricated either as colloids suspended in solution or as epitaxial structures grown on solid crystalline substrates. Epitaxial QDs can be reproducibly prepared, arranged in regular patterns, and directly incorporated into optoelectronic devices. QD nets may be fabricated in different sizes and a wide range of shapes, as pyramids, lenses, or flat cylinders. On the other hand, solution phase techniques provide exceptional control over size, monodispersity, and shape.[2] We may actually find a wide variety of shapes[3] from nearly spherical nanocrystals (NCs) to large aspect ratio nanorods (NRs) and tetrapods.[4] In addition, colloidal heteronanocrystals are also currently synthesized[5] as, e.g., core-shell dot-in-a-rod[6,7] and rod-in-a-rod.[8]

Elongated nanocrystals have an interesting physics, as systems located between zerodimensional QDs and one-dimensional quantum wires (QWs). They display unique characteristics including low lasing thresholds associated with increased Auger lifetimes,[9] large absorbance cross sections, and linearly polarized absorption and emission.[10] Their properties show promise for using NRs in applications such as lasing,[11] biolabeling,[12] polarized single-photon sources,[13] light harvesting, and carrier collection.[6,14]

Among semiconductor colloidal nanostructures, CdSe and CdS quantum dots and rods are excellent systems for optical and electronic applications due to their easy synthesis, optical quality, and relatively stable surface passivation. The band gaps of CdSe and CdS are in the visible light range and can be tuned by changing the nanostructure size. This makes them good candidates for optical related applications, including solar cells and photoelectrochemical cells.[15]

NRs can be coated with an epitaxial graded shell of a few monolayers in thickness.[16] This coating increases, in general, the NR stability in air and allows for better synthesis control and quality. In addition, this core/shell structures and nanojunctions are of special interest as the different band alignment can drive the electron and hole into different locations and dissociate the excitons, which is the main function of a p-n junction.[17]

Semiconductor nanocrystals are greatly impacted by the effects of strain arising in heterojunctions, in both the solid state phase and also in the colloidal state. On the one hand, lattice strain is the reason that QDs spontaneously grow on lattice mismatched solid substrates in the Stranski-Krastanov growth mode, leaving substantial residual strain in the nanocrystals. On the other hand, colloidal semiconductor (core)-shell materials, with a relevant mismatch in bond length between core and shell, can also generate a strong strain field in the nanocrystal, severely influencing its optical and electronic properties.[18] Thus, it has been reported that by varying the composition and size, CdSe/CdS heterostructured nanorods were tuned between type-I, quasi type-II, and type-II characteristics.[7,8]

In the present paper, we study the main characteristic strain trends arising in free-standing coated NRs. We have chosen CdSe/CdS as representative of II-IV coated NRs. Several issues are addressed. Among them the different aspect ratio, since buried QDs, look like flat cylinders or lens while NRs have a large aspect ratio like a cut nanowire. Also, we study the influence of the coating shell thickness, as NRs can be coated by one or a few monolayers (MLs) and, therefore, the strain at the border of the shell can be nonzero. In this case, we must impose boundary conditions of zero normal stress for the free NR surface, while in the case of a QD embedded in an infinite matrix, one assumes null deformation field far away from the QD border. We will see that beyond a rather small shell/system size ratio, the strain is similar to that of a QD buried in an infinite matrix. Since most of synthesized coated NRs are built of II-IV semiconductor materials, we write a code for hexagonal wurtzite crystal structure. As customary, we assume linear elasticity. With an appropriate input, the code can also be used for cubic zinc-blende or isotropic materials. We will carry out a comparative study of the strain distribution as obtained for hexagonal, cubic, and isotropic elasticities. Peeters *et al.*[19] reported that isotropic and

[a)]Electronic mail: josep.planelles@qfa.uji.es.

anisotropic cubic continuum mechanical models yield similar results, so that one can often employ simpler isotropic elasticity theory to estimate the strain in cubic crystals. We show here that this result can be extended in the sense that using appropriate elastic coefficients, all three models yield similar output. Finally, since NRs can be only partially coated,[3,5] we have also addressed the calculation of strain in partially buried systems. Also, we pay attention to the strain in the surrounding shell, as it is important for type-II systems.

II. THEORY

We have written a strain code for hexagonal wurtzite crystals whose volumetric elastic density energy reads[20]

$$e = \frac{1}{2}C_{xxxx}(\varepsilon_{xx}^2 + \varepsilon_{yy}^2) + \frac{1}{2}C_{zzzz}\varepsilon_{zz}^2 + C_{xxyy}\varepsilon_{xx}\varepsilon_{yy} + C_{xxzz}\varepsilon_{zz}(\varepsilon_{xx} + \varepsilon_{yy}) + 2C_{xzxz}(\varepsilon_{yz}^2 + \varepsilon_{xz}^2) + 2C_{xyxy}\varepsilon_{xy}^2, \quad (1)$$

where $C_{xyxy} = (C_{xxxx} - C_{xxyy})/2$ and the rest of elastic modulus tensor elements are linear independent. See supplementary material for details on the underlying theory, precise prescription employed for finite differences and implementation.[25] As for the boundary conditions, in short, if the dot is embedded in an infinite matrix, we assume a zero deformation field u far away from the dot border, i.e., $u = 0$ at the grid border and beyond. In the case of a dot coated (or partially coated) by finite shells, boundary conditions of zero normal stress for the free surface are employed. These are implemented by setting $\sum_j \sigma_{ij} n_j = 0$, where $\sigma_{ij} = \sum_{kl} C_{ijkl}\varepsilon_{kl}$ is the stress tensor at the border nodes and **n** is the outward normal to the border surface at these nodes.

Only three elastic modulus tensor elements remain linear independent for cubic zinc-blende symmetry. By replacing C_{zzzz} by C_{xxxx}, C_{xxzz} by C_{xxyy}, and C_{xzxz} by C_{xyxy} in Eq. (1) we formally reach the zinc-blende volumetric elastic density energy expression. Also, instead of the two different wurtzite lattice constants (*a, a, c*), zinc-blende has only a distinct lattice constant: (*a, a, a*). In turn, isotropic bodies require just two elastic coefficients, one related to hydrostatic compression (λ) and another to shear (μ). They are called Lamé coefficients. In terms of these coefficients, the elastic modulus tensor elements for an isotropic material read $C_{ijkl} = \lambda\delta_{ij}\delta_{kl} + \mu(\delta_{ik}\delta_{jl} + \delta_{il}\delta_{jk})$. Hence, just by writing an appropriate input, the wurtzite code can also be used for zinc-blende or isotropic materials.

Since strain distribution is invariant to the system scaling,[21] for a given core-shell system it is the size ratio shell/core which determines the strain strength.

III. RESULTS AND DISCUSSION

We analyze the components of the strain tensor for a series of CdSe/CdS heterostructures with different sizes and aspect ratios. The schematic structure is depicted in Fig. 1, namely, a CdSe cylinder of radius R and length L concentrically embedded in a CdS cylinder. The thicknesses of the CdS shell in the radial and longitudinal direction are S_1 and S_2, respectively. Unless otherwise stated, a wurtzite crystal lattice is considered. The elastic and lattice constants employed in the calculations[22] are summarized in Table I.

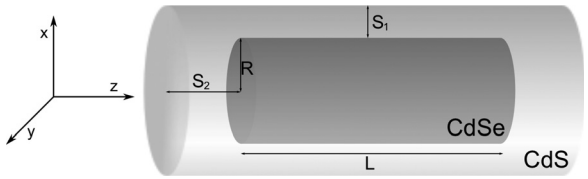

FIG. 1. Schematics of the studied nanostructures.

We start by focusing on the strain distributions of systems with different aspect ratio. The aim is to show the different behavior of the typically flat QDs obtained through physical growing methods and the chemically synthesized elongated nanorods. To this end, we show in Fig. 2 shading contour representations of the strain for four core-shell nanostructures with different aspect ratio. We plot the x - z cross section of the nanostructures for $y = 0$ (see Fig. 1). The inner CdSe nanostructure dimensions (R and L) and aspect ratio ($a.r. = L/2R$) are given on top of each column. In all cases we consider a CdS shell with a constant thickness of $S_1 = S_2 = 2$ nm.

Diagonal components of the strain tensor are represented in the first two rows of Fig. 2. ε_{xx} and ε_{yy} have been grouped in the so-called lateral strain, defined as $\varepsilon_{\parallel} = \frac{1}{2}(\varepsilon_{xx} + \varepsilon_{yy})$,[19] which assesses the strain along the radial direction of the cylinder. Due to the symmetry of the system, all off-diagonal components of the strain tensor except ε_{xz} are zero in the $y = 0$ plane. Then, we include ε_{xz} in Fig. 2. Also, the hydrostatic strain $\varepsilon_H = \varepsilon_{xx} + \varepsilon_{yy} + \varepsilon_{zz}$ is included.

From Fig. 2 we can see that ε_H and ε_{xz} undergo little changes versus the aspect ratio. The figure shows that ε_H is compressive in the core and nearly zero in the shell while ε_{xz} has only relevant values near the core edges. Significative changes versus the aspect ratio can be seen for lateral $\varepsilon_{\parallel}$ and ε_{zz} strain components, although their sum, ε_H, remains nearly unchanged. Then, since the wurtzite crystals deformation potentials for both the conduction and valence bands are anisotropic, the influence of strain on the energy structure can vary with changes in the aspect ratio, despite de constancy of the hydrostatic strain ε_H. This is particularly noticeable for the conduction band for which an isotropic hydrostatic deformation potential would lead to a nearly constant potential in the Hamiltonian, as the hydrostatic strain ε_H is almost independent of the aspect ratio, as can be seen in Fig. 2. We can see in this figure that large aspect ratios imply nearly zero lateral strain $\varepsilon_{\parallel}$ and strongly compressive ε_{zz} in the core and, nearly zero $\varepsilon_{\parallel}$ and slightly expansive ε_{zz} in the lateral part of the shell. Their sum, ε_H, is strongly compressive in the core and zero in the shell. All the same, small aspect ratios involve strongly compressive $\varepsilon_{\parallel}$ and expansive ε_{zz} in the core

TABLE I. Material parameters of wurtzite CdSe and CdS employed in the calculations.[22]

	C_{xxxx}	C_{xxyy}	C_{xxzz}	C_{zzzz}	C_{xzxz}	C_{xyxy}	a(Å)	c(Å)
CdSe	7.41	4.52	3.89	8.43	1.34	1.45	4.2999	7.0109
CdS	8.65	5.40	4.73	9.44	1.50	1.63	4.1348	6.749

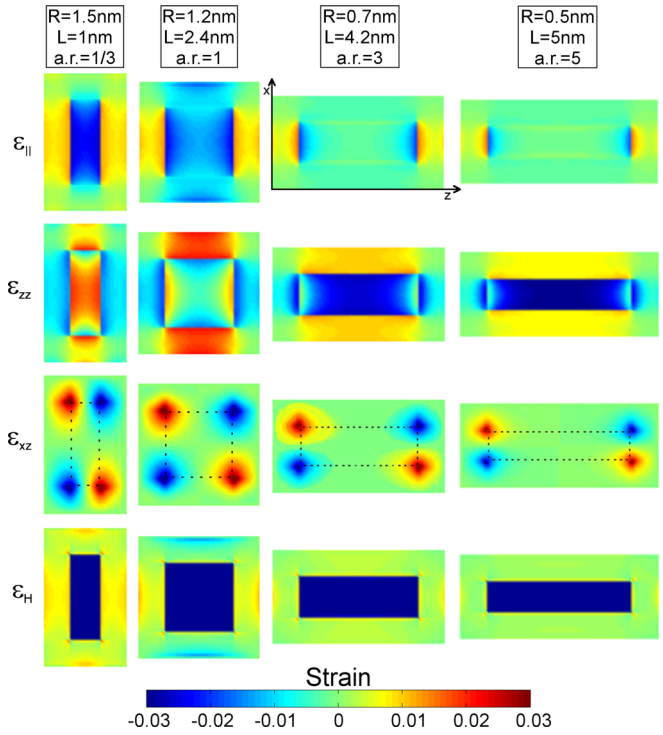

FIG. 2. (Color online) 2 D contours (x-z cross section at $y=0$, see Fig. 1) of the strain components for different aspect ratios. Geometries of the CdSe core and aspect ratios are included at the top of each column. A constant CdS shell thickness $S_1=S_2=2$ nm has been considered in all cases.

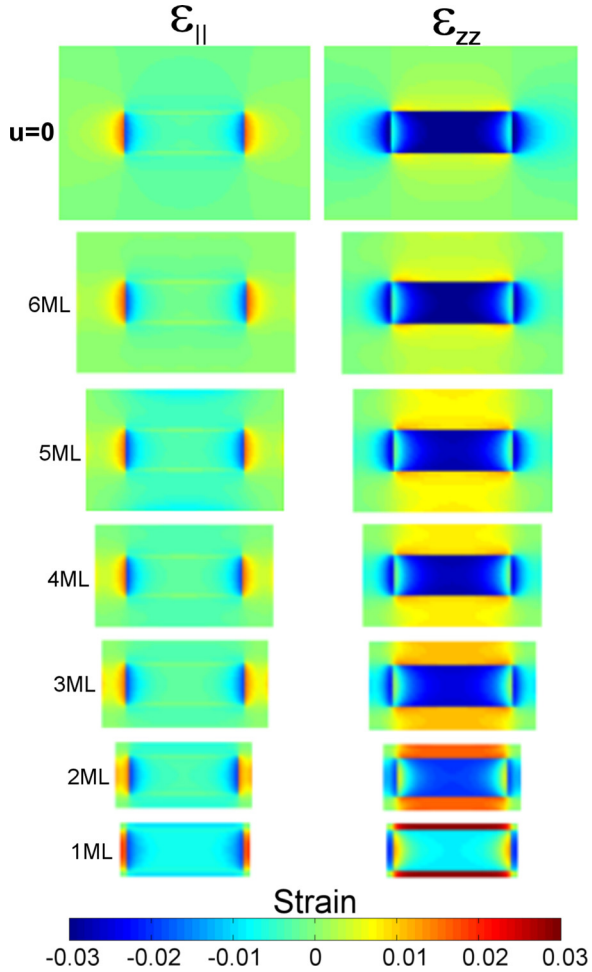

FIG. 3. (Color online) Diagonal strain components of a core-shell NR with different shell thickness. The CdSe core has a radius and length of $R=0.7$ nm and $L=4.2$ nm. The shell thickness is the same in all directions, ($S_1=S_2$), and its value is indicated in the left side of the panels in monolayers units (1 ML $=0.3$ nm). The topmost panels correspond to the case of a CdSe core buried in an infinte CdS matrix. We label it with $u_i=0$.

and softer with opposite sign in the shell. The sum ε_H is just strong compressive in the core.

Next we study the influence of the thickness of the coating shell. To this end, we fix the geometry of the CdSe core and cover it with an increasing number of CdS MLs. We assume that 1 ML $=0.3$ nm. The results are summarized in Fig. 3, where only the components $\varepsilon_{||}$ and ε_{zz}, which undergo the most significative changes, are included. Also, as a reference, the case of a core buried in an infinite CdS matrix is included. We label it in the figure with $u=0$, reminding the boundary conditions imposed in this case. The core geometry is defined by $R=0.7$ nm and $L=4.2$ nm (see schematic in Fig. 1). The lateral S_1 and vertical S_2 shell thickness are equal in these series of calculations.

The main result one can see in Fig. 3 is that while after covering the core with a few MLs the strain resembles that of a core buried in an infinite matrix, severe differences occur for typically synthesized[5] 1-2 ML thick core-shells. Especially noticeable is the strong expansive ε_{zz} in the shell, the can be of relevance for type II systems, and the expected reduction of compressive ε_{zz} in the core, which is paralleled by some increase of compressive $\varepsilon_{||}$.

In order to complete this study, we fix next the size S_2 of the shell at the two ends of the core and change the lateral shell thickness S_1 from a uniform covering $S_1=S_2$ up to a null $S_1=0$ lateral coating. The results are summarized in Fig. 4, where again, only $\varepsilon_{||}$ and ε_{zz} are represented. As we can see in the figure, a well covered core has a negligible lateral $\varepsilon_{||}$ strain in both core and shell, except in a region very close to the two core ends. Meanwhile, ε_{zz} is strongly compressive in the core and softly expansive in the shell, except close to the two core ends where it is compressive. The hydrostatic strain $\varepsilon_H=\varepsilon_{||}+\varepsilon_{zz}$ being compressive in the core and nearly zero in all the shell (not shown).

Also, trends similar to those in Fig. 3 of strong changes as we reduce the lateral S_1 covering, can be seen in Fig. 4. On the one hand, the strain in the shell, at the two ends of the core, is negligible except in the regions next to the core/shell interfaces. On the other hand, a strong ε_{zz} expansion paralleled by a $\varepsilon_{||}$ compression in the lateral shell can be seen.

As far as the core is concerned, the reduction of S_1 turns into a less severe ε_{zz} compression. A noticeable jump in properties is produced after removing the last lateral covering ML. On the one hand, compressive ε_{zz} turns into expansive. In parallel, $\varepsilon_{||}$ goes from soft to strongly compressive, so that their sum, the hydrostatic strain ε_{H}, results compressive. Regarding the core hydrostatic strain, the change produced by eliminating the lateral covering ML by ML up to $S_1=0$ is gradual. However, since wurtzite deformation potentials associated with $\varepsilon_{||}$ and ε_{zz} are different, a severe strain-induced change in the electronic structure is expected by removing the lateral core coating.

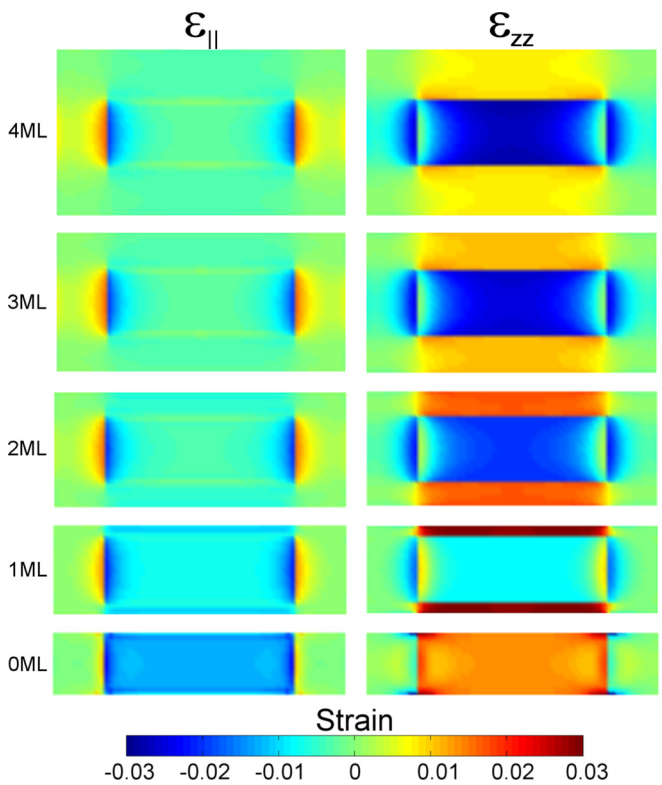

FIG. 4. (Color online) Diagonal strain components of a core-shell NR as the shell thickness in the lateral direction (S_1) is reduced while it is fixed in the longitudinal direction ($S_2 = 4$ ML). The radius and length of the core are $R = 0.7$ nm and $L = 4.2$ nm.

Tadic *et al.*[19] showed that the strain distribution of a flat cylinder buried in a matrix is almost the same for an internal material symmetry isotropic or cubic (Zinc-Blende). We next extend their study to hexagonal symmetry (wurtzite) and elongated cores coated with just a few MLs of covering material. We consider here a CdSe core defined by a radius and length of $R = 0.7$ nm and $L = 4.2$ nm, respectively (see Fig. 1), and calculate the strain using the proper wurtzite elastic modulus tensor parameters (see Table I) and also related cubic and isotropic coefficients. Since by formally replacing the elastic coefficient C_{zzzz} by C_{xxxx}, C_{xxzz} by C_{xxyy}, and C_{xzxz} by C_{xyxy} in Eq. (1), and c by a in the lattice constants, we turn hexagonal wurtzite into cubic zinc-blende, according to Eq. (1), the elastic and lattice constants of the zinc-blende closest to the wurtzite material must be $C^{znbl}_{xxxx} = (2C^{wr}_{xxxx} + C^{wr}_{zzzz})/3$, $C^{znbl}_{xxyy} = (C^{wr}_{xxyy} + 2C^{wr}_{xxzz})/3$, $C^{znbl}_{xyxy} = (C^{wr}_{xyxy} + 2C^{wr}_{xzxz})/3$, and $a^{znbl} = \sqrt[3]{(a^{wr})^2 c^{wr}}$. We use geometric average for the lattice constant in order to get a new unit cell with the same volume as the former one.

The general formula for the elastic coefficients of isotropic materials in terms of the two Lamé λ and μ coefficients, $C_{ijkl} = \lambda\delta_{ij}\delta_{kl} + \mu(\delta_{ik}\delta_{jl} + \delta_{il}\delta_{jk})$, particularize to $C_{xxxx} = \lambda + 2\mu$, $C_{xxyy} = \lambda$, and $C_{xzxz} = \mu$. This represents an extra restriction on zinc-blende elastic coefficients: $C_{xxxx} = C_{xxyy} + 2C_{xzxz}$. Then, in order to find the isotropic material elastic coefficients C^{iso}_{ijkl} closest to zinc-blende ones C^{znbl}_{ijkl}, we write $C^{iso}_{ijkl} = C^{znbl}_{ijkl} + \Delta C^{znbl}_{ijkl}$, with $ijkl = xxxx, xxyy, xyxy$, and calculate those isotropic coefficients that yield the minimum of the sum $(\Delta C^{znbl}_{xxxx})^2 + (\Delta C^{znbl}_{xxyy})^2 + (\Delta C^{znbl}_{xyxy})^2$ subject to the restrictions $C^{iso}_{xxxx} = C^{iso}_{xxyy} + 2C^{iso}_{xzxz}$, i.e., $C^{znbl}_{xxxx} - C^{znbl}_{xxyy} - 2C^{znbl}_{xzxz} = \Delta C^{znbl}_{xxxx} - \Delta C^{znbl}_{xxyy} - 2\Delta C^{znbl}_{xzxz} = k$. It yields $C^{iso}_{xxxx} = C^{znbl}_{xxxx} - k/6$, $C^{iso}_{xxyy} = C^{znbl}_{xxyy} + k/6$, and $C^{iso}_{xyxy} = C^{znbl}_{xyxy} + k/3$. We use these coefficients when calculating within the isotropic approximation.[23]

In order to better show quantitative differences among the models, profiles along the main axes corresponding to the three models instead of two-dimensional shading contour representations are displayed in Fig. 5. In addition, for the sake of comparison, actual cubic coefficients for Zinc-Blende CdSe and CdS materials[22] are employed in a fourth series of calculations and the results included in the figure (dotted lines).

A neat result emerges in Fig. 5: with appropriate related elastic parameters, isotropic, cubic, and hexagonal models for the elastic energy lead to almost identical strain profiles, thus extending the conclusions by Tadic *et al.*[19] to elongated systems and wurtzite structure. Note, however, that the actual elastic modulus tensor of the Zinc-Blende materials and the cubic approximation obtained from the elastic parameters of its polymorphic wurtzite conterpart are different and yield different strain profiles (see dotted versus dashed lines in Fig. 5). One may conclude that, with the above prescription for the isotropic approximation to an hexagonal crystal, the simple model proposed by David[24] can safely be used to estimate strain in elongated, few ML covered wurtzite NRs.

IV. SUMMARY AND CONCLUSIONS

We study the main characteristic strain trends of free standing coated NRs related to aspect ratio and shell thickness. The results reveal that while hydrostatic strain ε_H is almost independent of the aspect ratio, $\varepsilon_{||}$ and ε_{zz} undergo severe changes versus it. As for the thickness of the coating shell, we see that after covering the NR core with a few MLs, the strain resembles that of a core buried in an infinite matrix. However, severe changes occur for thin shells of 1-2 ML thick. Finally,

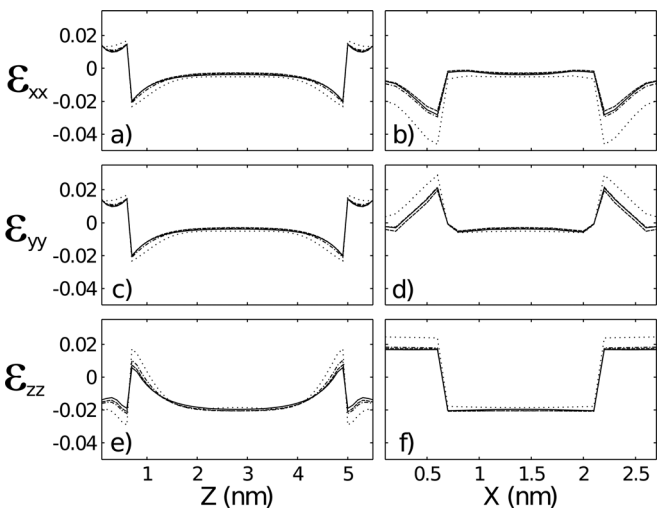

FIG. 5. Diagonal strain components profiles along the centered axial (left) and in-plane (right) axis for a system with $R = 0.7$ nm, $L = 4.2$ nm, and $S_1 = S_2 = 2$ ML, calculated with different models: wurtzite parameters (solid line), cubic approximation to these wurtzite parameters (dashed line), isotropic approximation (dashed dotted line), and actual zinc blend parameters (dotted line).

following the suggestion by Tadic *et al.*[19] that strain distribution of flat cylinders buried in a matrix is almost the same for isotropic or cubic (Zinc-Blende) materials, we have extended their study to hexagonal symmetry (wurtzite) and elongated cores coated with just a few MLs of covering material and conclude that, with the appropriate parameters, isotropic, and hexagonal strain profiles are hardly distinguishable.

ACKNOWLEDGMENTS

We acknowledge continuous financial support from MCINN project CTQ2008-03344 and UJI-Bancaixa projects P1-1A2009-03 and P1-1B2011-01.

[1]L. Qi, Coord. Chem. Rev. **254**, 1054 (2010).
[2]A. M. Smith and S. Nie, Acc. Chem. Res. **43**, 190 (2010).
[3]C. de Mello Donega, Chem. Soc. Rev. **40**, 1512 (2011).
[4]D. J. Milliron, S. M. Hughes, Y. Cui, L. Manna, J. Li, L.-W. Wang, and A. P. Alivisatos, Nature **430**, 190 (2004).
[5]F. Shieh, A. E. Saunders, and B. A. Korgel, J. Phys. Chem. B **109**, 8538 (2005); B. Huo and B. A. Korgel, Nano Lett. **8**, 2490 (2008).
[6]D. V. Talapin, R. Koeppe, S. Götzinger, A. Kornowski, J. M. Lupton, A. L. Rogach, O. Benson, J. Feldmann, and H. Weller, Nano Lett. **3**, 1677 (2003).
[7]E. Yoskovitz, G. Menagen, A. Sitt, E. Lachman, and U. Banin, Nano Lett. **10**, 3068 (2010).
[8]A. Sitt, A. Salant, and U. Banin, Nano Lett. **11**, 2054 (2011).
[9]V. I. Klimov, J. Phys. Chem. B **110**, 16827 (2006); M. Kazes, D. Y. Lewis, Y. Ebenstein, T. Mokari, and U. Banin, Adv. Mater. **14**, 317 (2002).
[10]X. Chen, A. Nazzal, D. Goorskey, M. Xiao, Z. A. Peng, and X. G. Peng, Phys. Rev. B **64**, 245304 (2001).
[11]T. Y. Zhai, X. S. Fang, Y. S. Bando, Q. Liao, X. J. Xu, H. B. Zeng, Y. Ma, J. N. Yao, and D. Golberg, ACS Nano **3**, 949 (2009).
[12]S. Deka, A. Quarta, M. G. Lupo, A. Falqui, S. Boninelli, C. Giannini, G. Morello, M. De Giorgi, G. Lanzani, C. Spinella, R. Cingolani, T. Pellegrino, and L. Manna, J. Am. Chem. Soc. **131**, 2948 (2009).
[13]F. Pisanello, L. Martiradonna, P. Spinicelli, A. Fiore, J. P. Hermier, L. Manna, R. Cingolani, E. Giacobino, M. De Vittorio, and A. Bramati, Superlattices Microstruct. **47**, 165 (2010).
[14]R. D. Robinson, B. Sadtler, D. O. Demchenko, C. K. Erdonmez, L. W. Wang, and A. P. Alivisatos, Science **317**, 355 (2007).
[15]J. M. Spurgeon, H. A. Atwater, and N. S. Lewis, J. Phys. Chem. C **112**, 6186 (2008).
[16]L. Manna, E. Scher, L. Li, and A. Alivisatos, J. Am. Chem. Soc. **124**, 7145 (2002).
[17]Y. Luo and L.-W. Wang, ACS Nano **4**, 91 (2010).
[18]A. M. Smith and S. Nie, Acc. Chem. Res. **43**, 190 (2010); A. M. Smith A. M. Mohs, and S. Nie, Nat. Nanotechnol. **4**, 56 (2009).
[19]M. Tadic, F. M. Peeters, K. L. Janssens, M. Korkusinski, and P. Hawrylak, J. Appl. Phys. **92**, 5819 (2002); M. Tadic, F. M. Peeters, and K. L. Janssens, Phys. Rev. B **65**, 165333 (2002).
[20]L. D. Landau and E. M. Lifshitz, *Theory of Elasticity*, 3rd ed. (Pergamon, Oxford, 1986).
[21]B. Jogai, J. Appl. Phys. **88**, 5050 (2000).
[22]A. Sadao, *Handbook of Physical Properties of Semiconductors* (Kluwert Academic Group, Holand, 2004), Vol. 3.
[23]Note that in Ref. 19, comparison with isotropic elasticity was made for materials with a Poisson relation $\nu = 1/3$. Since, in terms of the Young modulus E and Poisson relation ν, the Lamé coefficients read $\lambda = \frac{\nu E}{(1+\nu)(1-2\nu)}$ and $\mu = \frac{E}{2(1+\nu)}$, for the particular case $\nu = 1/3$, it turns that $\lambda = 2\ \mu$, and therefore, that $C_{xxyy} = C_{xxxx}/2$ and $C_{xyxy} = C_{xxxx}/4$. Then, to check the isotropic approximation, one might employ the C_{xxxx} coefficient of a given material only and calculate any other in terms of it, as done in Ref. 19.
[24]J. H. David, J. Appl. Phys. **84**, 1358 (1998).
[25]See supplementary material at http://dx.doi.org/10.1063/1.3673256 for details on the underlying theory, precise prescription employed for finite differences and implementation.